Article:

Diaz, L., Butler, A., Avisar, D. et al. (Accepted: 2026) Disentangling Anthropogenic Effects on Southern Hemisphere Circulation and Surface Climate: a Multi-Model Large Ensemble Approach. Journal of Geophysical Research: Atmospheres. ISSN: 2169-897X (In Press)

Journal of Geophysical Research - Atmospheres

Supporting Information for

Disentangling Anthropogenic Effects on Southern Hemisphere Circulation and Surface Climate: a Multi-Model Large Ensemble Approach

Leandro B. Díaz[1,2,3]*, Amy H. Butler[4]*, David Avisar[5,6], Sabine Bischof [7], Chloe L. Boehm[8], Ghyslaine Boschat[9,10], William J. Dow[11], Chaim I. Garfinkel[5], Kevin M. Grise[12], Hemant Khatri[13], Bianca Mezzina[14], Marisol Osman[1,2,3], Jonathon S. Wright[15], Panos J. Athanasiadis[16], Julie M. Arblaster[17,10], Erik Behrens[18], Thomas J. Bracegirdle[19], Yuanrui Chen[15], Eun-Pa Lim[9,10], Amanda C. Maycock[11], Seung-Ki Min[20], Julia Mindlin[21], Scott M. Osprey [22,23], Michael Sigmond[24], Doug Smith[13] and Tiffany Shaw[25]

[1]Universidad de Buenos Aires. Facultad de Ciencias Exactas y Naturales. Departamento de Ciencias de la Atmósfera y los Océanos (DCAO). Buenos Aires, Argentina.

[2]CONICET – Universidad de Buenos Aires. Centro de Investigaciones del Mar y la Atmósfera (CIMA). Buenos Aires, Argentina.

[3]Instituto Franco-Argentino de Estudios sobre el Clima y sus Impactos (IFAECI) – IRL 3351 – CNRS-CONICET-IRD-UBA. Buenos Aires, Argentina.

[4]NOAA Chemical Sciences Laboratory, Boulder, CO, United States.

[5]Fredy & Nadine Herrmann Institute of Earth Sciences, The Hebrew University of Jerusalem, Jerusalem, Israel.

[6]The Department of Applied Mathematics, Israel Institute for Biological Research, Ness-Ziona, Israel.

[7]GEOMAR Helmholtz Centre for Ocean Research Kiel.

[8]Department of Atmospheric Science, Colorado State University, Fort Collins, CO, United States.

[9]Bureau of Meteorology, Melbourne, Victoria, Australia.

[10]ARC Special Research Initiative for Securing Antarctica's Environmental Future, Clayton, Victoria, Australia.

[11]School of Earth and Environment, University of Leeds, Leeds, UK.

[12]Department of Environmental Sciences, University of Virginia, Charlottesville, VA, USA.

[13]Met Office Hadley Centre, Exeter, United Kingdom.

[14]Earth and Climate Research Center, Earth and Life Institute, Université catholique de Louvain, Louvain-la-Neuve, Belgium.

[15]Department of Earth System Science, Institute for Global Change Studies, Ministry of Education Key Laboratory for Earth System Modeling, Tsinghua University, Beijing.

[16]CMCC Foundation - Euro-Mediterranean Center on Climate Change, Bologna, Italy.

[17]School of Earth, Atmosphere and Environment, Monash University, Clayton, Victoria, Australia.

[18]Earth Sciences New Zealand, Wellington, New Zealand.

[19]British Antarctic Survey, Cambridge, United Kingdom.

[20]Division of Environmental Science and Engineering, Pohang University of Science and Technology, Pohang, South Korea.

[21]Leipzig University.

[22]National Centre for Atmospheric Science, University of Oxford, Oxford, UK.

[23]Atmospheric, Oceanic and Planetary Physics, University of Oxford, Oxford, UK.

[24]Canadian Centre for Climate Modelling and Analysis, Environment and Climate Change Canada, Victoria, BC, Canada.

[25]The University of Chicago.

Contents of this file

Introduction

In the Supporting Information, we show details which are not shown in the main manuscript about the data used for ocean and sea ice variables, as well as additional figures.

Text S1.

The availability of ocean variables as the ones used for this study - sea surface temperatures, downward heat flux at the sea water surface, sea water potential temperature - are more restricted than for standard atmospheric variables in LESFMIP simulations. Thus, ocean diagnostics were computed using only the ensemble members listed in Table S1 that included all three ocean variables, which were used to create Figures 8 and 10. Similarly, some members were not available for the sea ice diagnostics. Table S2 lists the number of members used to create Figures 11 and S5.

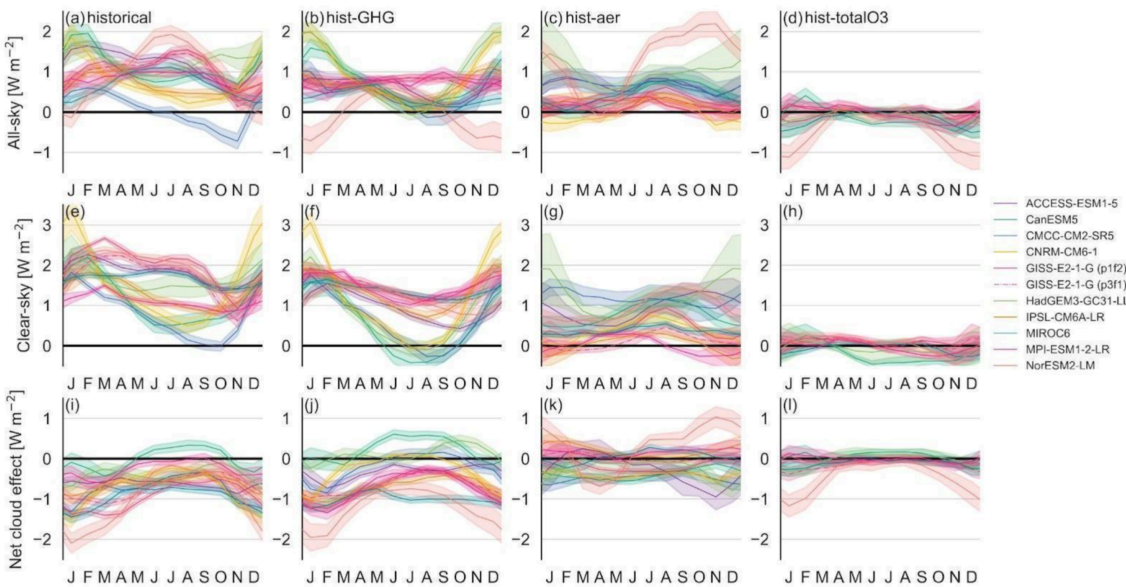

Figure S1. Seasonal cycles of the difference in (a)-(d) all-sky top-of-atmosphere (TOA) energy imbalance between the 1980-2014 mean (for each ensemble independently) and the 1850-1884 mean (aggregated over the hist-GHG, hist-aer, and hist-totalO3 ensembles only) and its (e)-(h) clear-sky and (i)-(l) cloud radiative effect components. Results are shown for the (far left: a, e, i) historical, (center left: b, f, j) hist-GHG, (center right: c, g, k) hist-aer, and (far right: d, h, l) hist-totalO3 ensembles. For each model, ensemble spread is illustrated by the standard deviation across the ensemble. The two variants of the GISS-E2-1-G model are shown to more accurately reflect the spread produced by this model, where the p1f2 variant corresponds to prescribed aerosol and p3f1 to interactive aerosol (Miller et al. 2020). Although the y-axis range is shifted for each of the three rows, its range is fixed to 4 W m^{-2} in all panels to enable comparison.

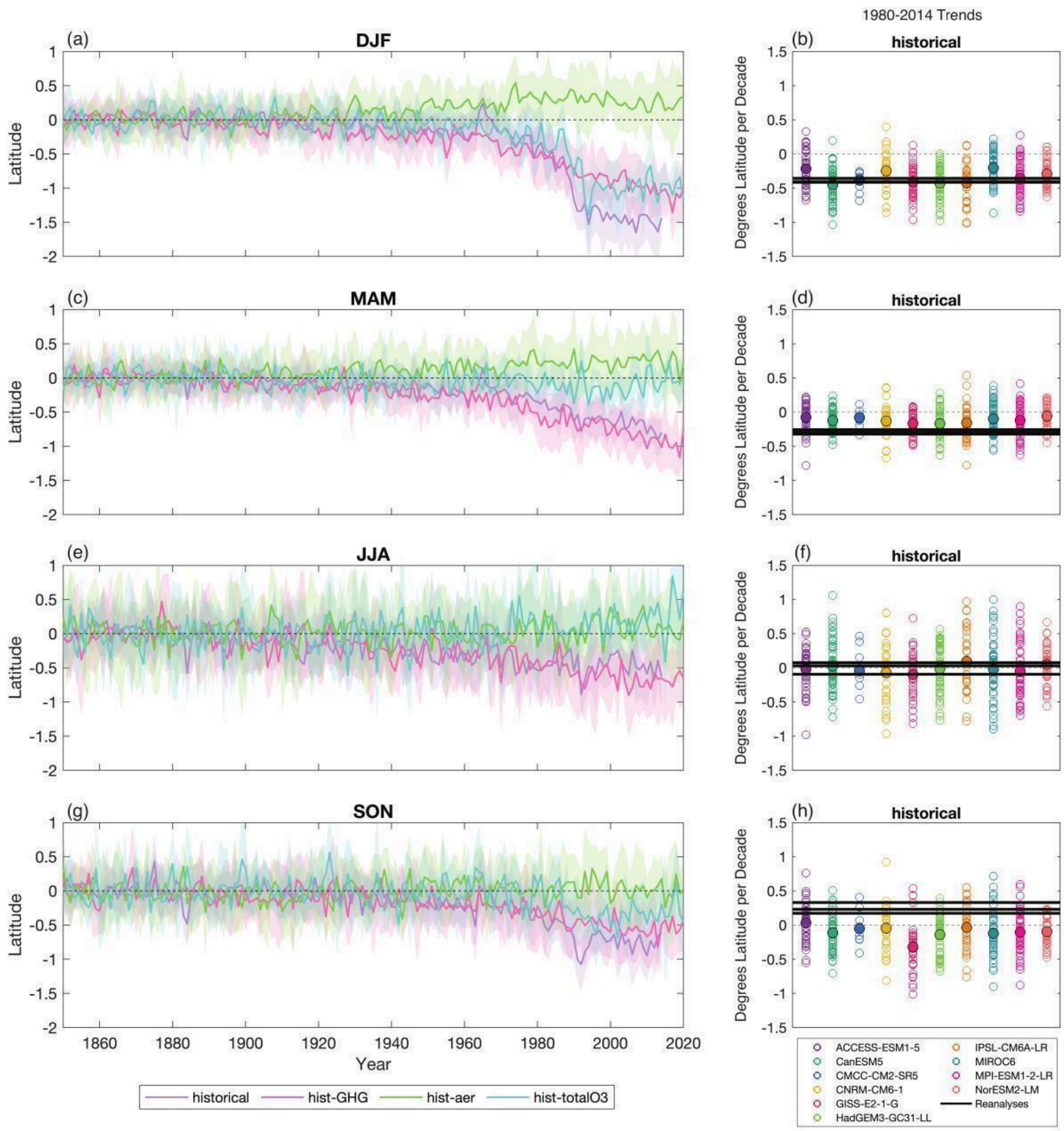

Figure S2. SH eddy-driven jet latitude year-to-year variabilities and long-term trends. Left column: Multi-model mean time series (1850–2020) of the four experiments (historical , hist-GHG , hist-aer and hist-totalO3) for each season (DJF, MAM, JJA, SON). Values relative to 1850–1884 period. In each case, the shading indicates ±1 standard deviation across model ensemble means. Right column: Linear trends over 1980–2014 for historical experiment for each season (DJF, MAM, JJA, SON). Open circles represent individual ensemble members, filled circles show model ensemble means, and horizontal lines indicate trends from ERA5, MERRA2, and JRA55 reanalyses.

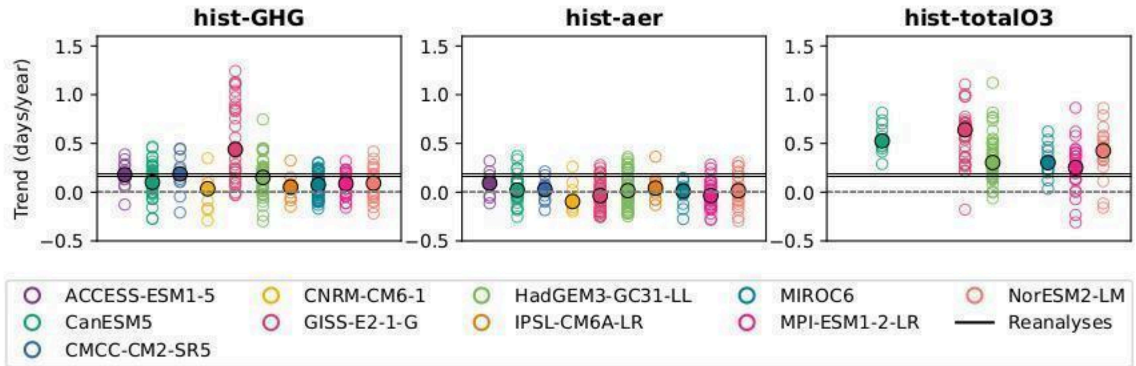

Figure S3. Linear trends for final stratospheric warming (FSW) date over 1980–2013 for (a) hist-GHG, (b) hist-aer and (c) hist-totalO3 experiments. Open circles represent individual ensemble members and filled circles show model ensemble means.

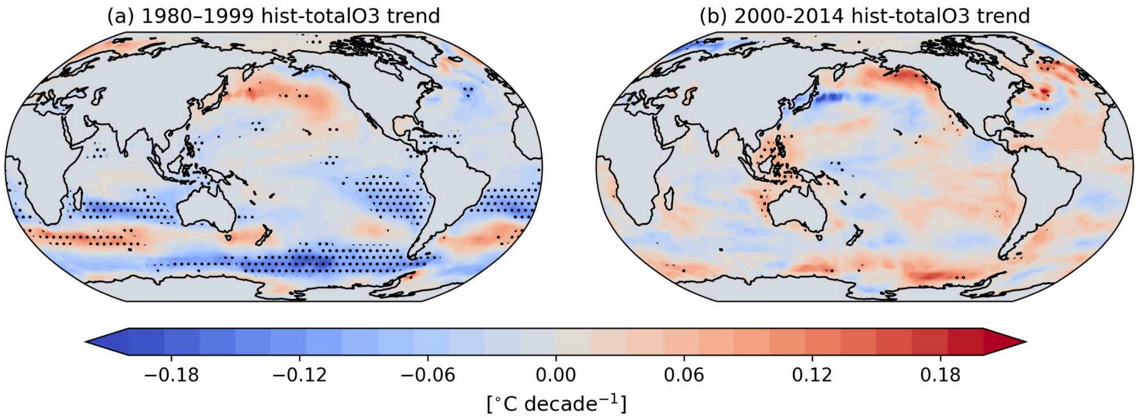

Figure S4. Multi-model mean DJF sea surface temperature (SST) trends from hist-totalO3 experiment for (a) 1980-1999 and (b) 2000-2014 periods. Units in ºC per decade. The stippling indicates regions where all models agree on the sign. The included models are those for which simulations were available from all experiments (CanESM5, GISS-E2-1-G, HadGEM3-GC31-LL, MIROC6, MPI-ESM1-2-LR and NorESM2-LM), and the number of ensemble members listed in Table 1 was used.

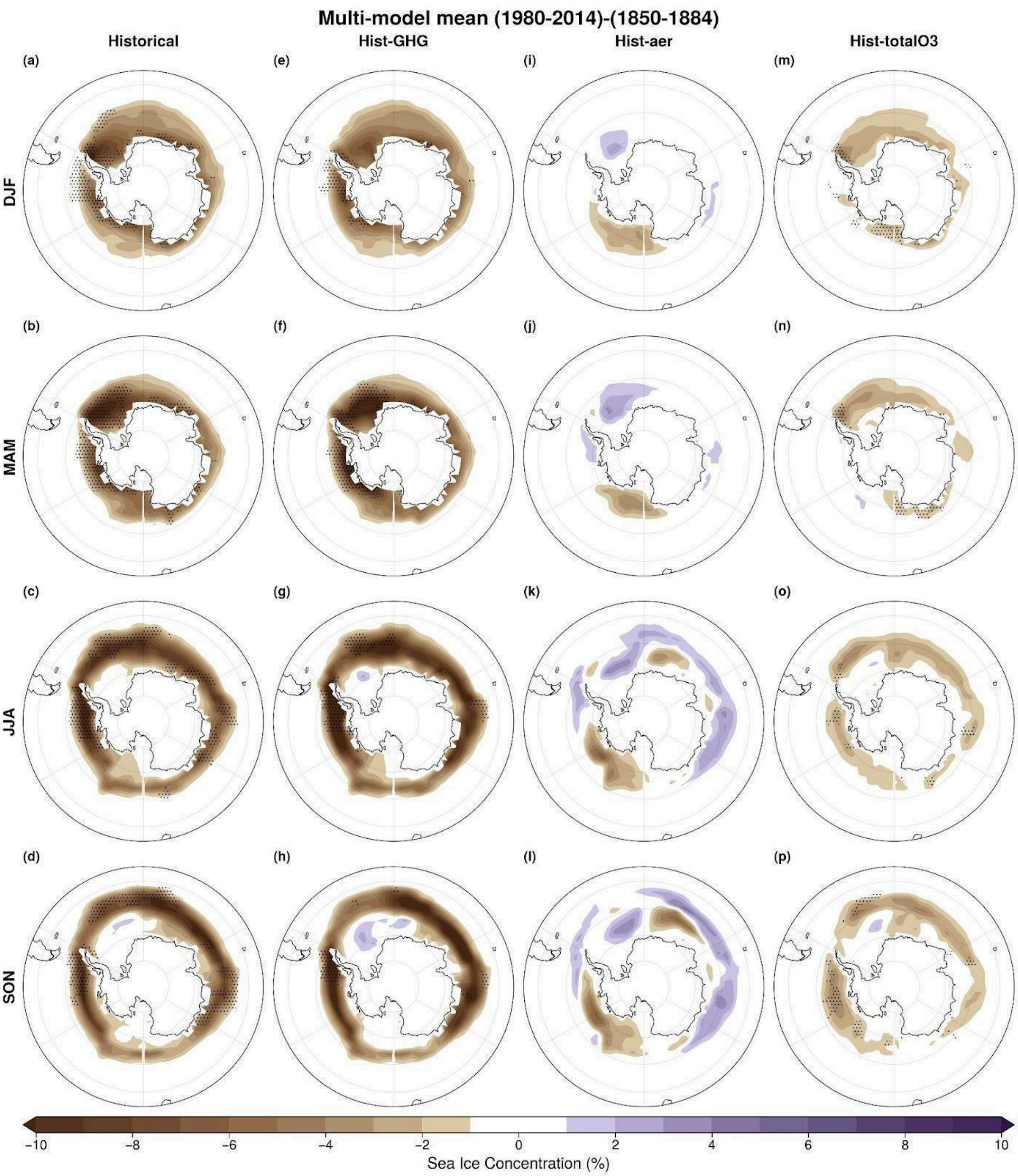

Figure S5: Multi-model mean sea ice concentration (SIC) response (difference between 1980–2014 and 1850–1884 periods) for (top row) DJF, (second row) MAM, (third row) JJA, and (bottom row) SON, for the (left column) historical, (second column) hist-GHG, (third column) hist-aer, and (right column) hist-totalO3 experiments. The stippling indicates regions where all models agree on the response sign. Note that sea ice variables for some ensemble members for a number of models were not available. For details, see Text S1 and Table S2.

Model	Experiments			
	historical	hist-GHG	hist-aer	hist-totalO3
ACCESS-ESM1-5	40	9	8	-
CanESM5	64	50	30	10
CMCC-CM2-SR5	10	10	10	-
CNRM-CM6-1	30	3	3	-
GISS-E2-1-G	36	39	36	5
HadGEM3-GC31-LL	55	55	55	50
IPSL-CM6A-LR	10	10	10	-
MIROC6	10	-	-	-
MPI-ESM1-2-LR	50	30	30	30
NorESM2-LM	3	3	3	-

Table S1. LESFMIP models, experiments and number of members used for Figures 8 and 10.

Model	Experiments			
	historical	hist-GHG	hist-aer	hist-totalO3
ACCESS-ESM1-5	40	9	10	-
CanESM5	65	50	30	10
CMCC-CM2-SR5	10	10	10	-
CNRM-CM6-1	21	10	10	-
GISS-E2-1-G	46	40	40	39
HadGEM3-GC31-LL	55	55	55	50
IPSL-CM6A-LR	33	10	10	-
MPI-ESM1-2-LR	50	30	30	30
NorESM2-LM	40	20	20	20

Table S2. LESFMIP models, experiments and number of members used for sea ice diagnostics.